JREE: Vol. 7, No. 4, (Autumn 2020) 30-43

Journal of Renewable Energy and Environment

Research Article

Journal Homepage: www.jree.ir

Adaptive Robust Control Design to Maximize the Harvested Power in a Wind Turbine with Input Constraint

Hossein Dastres, Ali Mohammadi, Behrooz Rezaie*

Department of Electrical and Computer Engineering, Babol Noshirvni University of Technology, P. O. Box: 47148-71167, Babol, Mazandaran, Iran.

PAPER INFO

Paper history:
Received 17 April 2020
Accepted in revised form 02 August 2020

Keywords:
Second-Order Sliding Mode Control,
Fast Integral Terminal Sliding Mode Control,
Input Saturation,
Maximum Power Point Tracking

ABSTRACT

This paper deals with the problem of maximizing the extracted power from a wind turbine in the presence of model uncertainties and input saturation. An adaptive second-order integral terminal sliding mode speed control method is utilized to address this problem. The presented method benefits from the advantages of several control techniques, i.e., adaptability, robustness, finite-time convergence, and the capability of coping with the input saturation. The robust nature of the designed controller causes its high performance in facing the uncertainties in the wind turbine model. In this paper, to compensate for the effect of input saturation, an auxiliary dynamic variable is added to the tracking error and also an adaptation law is designed so that the finite-time convergence of the closed-loop system can be achieved. Moreover, to reduce the mechanical stresses which are the result of the chattering phenomenon, a second-order sliding surface is employed. The finite-time convergence of the designed controller has been proven by the Lyapunov stability theorem in which the finite-time convergence of the tracking error to zero is guaranteed. Finally, to illustrate the effectiveness and satisfactory performance of the proposed controller, two comparative simulations are carried out. The results of this comparison show that the proposed controller has less error to track the optimal speed and when the model uncertainties and input saturation occur in the wind turbine system, the proposed controller is almost 3 % more efficient than the existing controllers.

https://doi.org/10.30501/jree.2020.224180.1093

1. INTRODUCTION

Using renewable energy sources such as wind, sea waves and solar systems have been intensely growing in recent years. These energy sources are great alternatives for other sources of energy which are mainly based on fossil fuels. Wind energy is an attractive resource which has received a great amount of attention because it is clean and also commonplace [1]. Two important and main objectives in the harvesting of the wind power are first, the extraction of the maximum power of the wind and second the reduction of the mechanical stress on the wind turbine. These two goals can be achieved thanks to the control strategies that are developed for various operation regions of the wind turbines. As shown in Fig. 1 four different operation regions can be defined for power extraction of the wind, using variable speed wind turbines (VSWTs). Regions 1 and 4 are in the middle of the cut-in and cut-out wind speed. Since the extracted wind power, is less than the losses in this state, it is necessary to turn-off the turbine and disconnect it from the grid in Region 1. However, in Region 4, the wind speed is so high that, the wind turbine may get damaged; hence, the wind turbine should be turned off. In Region 2, the wind speed is between the cut-in and nominal wind speed; in this region, the maximum power point tracking (MPPT) strategy is implemented to extract the maximum power from the wind power. In a wind turbine, the generator torque and the pitch angle are used to control the wind turbine velocity. To harvest the maximum power, in Region 2 the torque of the generator is used as the control input and the blade pitch, is considered to be constant. Region 3 is between the nominal and cut-out speed of the wind and to prevent the turbine to get damaged the pitch angle is used to control the system for regulating the wind turbine power at its rated value [2, 3]. In the literature, to control the harvested energy of the wind in VSWT, linear control methods like proportional-integral (PI), proportional-integral-derivative (PID) [4, 5], linear robust control [6-7], linear-quadratic (LQ) and linear-quadratic-Gaussian (LQG) [8-9] have been proposed. In these methods, the wind turbine model, is considered to be linear, however, in the wind turbine system there are unknown disturbance sources, uncertainties and highly nonlinear terms and the proposed methods cannot guarantee the robustness of the closed-loop system against these problems. When uncertainties and disturbances have high variations, these methods not only have poor performances, but also the stability of the closed-loop system cannot be guaranteed and also high precise results cannot be achieved [1, 3, and 10].

In order to make sure that the wind turbine system is stable in the presence of nonlinearities, uncertainties and disturbances, some of the more efficient nonlinear methods like sliding mode control (SMC) [3, 11], adaptive backstepping control [12] and robust nonlinear control [13] have been implemented. In [3], a sliding mode controller has been designed for maximizing the extracted power in a large scale variable speed wind turbine. In [11], an integral sliding mode controller and a PI controller have been designed for Regions 2 and 3 respectively, so that the generator torque is

*Corresponding Author's Email: brezaie@nit.ac.ir (B. Rezaie)
URL: http://www.jree.ir/article_111286.html

Please cite this article as: Dastres, H., Mohammadi, A. and Rezaie, B., "Adaptive robust control design to maximize the harvested power in a wind turbine with input constraint", ***Journal of Renewable Energy and Environment (JREE)***, Vol. 7, No. 4, (2020), 30-43.

used to maximize the harvested power and the pitch angle is used to keep the wind turbine power at its rated power. Reference [12] presents a control scheme for a doubly-fed induction generator (DFIG) which is based on the adaptive pole placement control method which is an extension of the backstepping control method. To improve the output wind turbine power and also take into account the unknown disturbance sources and uncertainties, robust H∞ controller in combination with a PID controller has been presented in [14]. In [15], a neural network-based adaptive controller for Region 2 and 3 is designed so that the smooth transition between two modes can be ensured and the Radial-Basis-Function (RBF) Neural Network (NN) estimator is also utilized to approximate the uncertainties and disturbances in an adaptive control method. In this method to achieve the asymptotically stability, a restrictive assumption has been made on the wind turbine speed. Chattering problem, poor performance against the model parameter variation, low ability in the disturbance rejection and the lack of asymptotic stability are the disadvantages of these methods, respectively.

It is well known that the SMC method is robust against the different types of uncertainties and disturbances. However, it is not very sensitive to the variation of the system parameters.

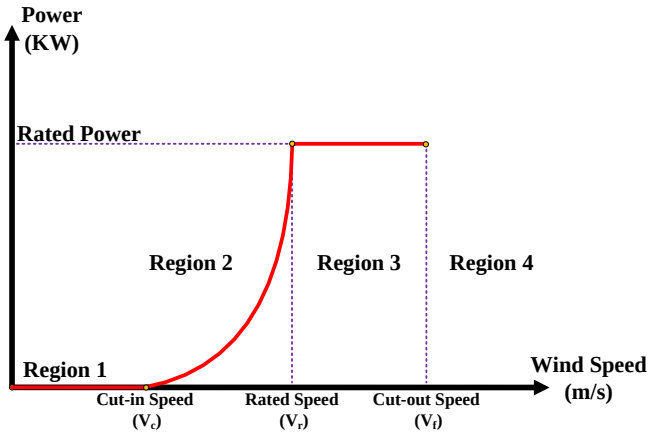

Figure 1. Four operating regions of wind turbine.

Therefore, this method has been developed for a variety of systems like power systems [16], electrical machines [17] and spacecrafts [18]. Since, in the wind turbine system, many dilemmas such as nonlinear sources, disturbances and parameter uncertainties exist, so by applying this controller to the wind turbine, satisfactory results can be achieved. There are two important steps in the SMC method which include: (a) selecting a suitable sliding surface; (b) designing the control input so that the system state variables reach to the sliding surface. In the traditional SMC method, only asymptotic stability can be provided and the convergence of the tracking error to zero will not be ensured in the finite time [19]. In the second region, to improve the maximum extraction of the wind power, an optimal speed for rotor is needed. Hence, by exploiting large control effort, it is possible to obtain a faster convergence in control schemes with high precision, which is severely adverse in practical applications. However, implementing the terminal SMC (TSMC) with nonlinear terminal sliding surface can be a proper solution for the aforementioned problem. In the TSMC method, near the equilibrium point of the system, the singularity problem occurs and non-singular TSMC (NTSMC) can solve this problem [20]. Moreover, the chattering phenomenon appears if the TSMC approach is implemented and it is because of the excitation of unmodeled dynamics of the system with high frequency which causes actuators to get damaged [21]. A conventional technique to reduce the chattering phenomenon is substituting the sign function with saturation or sigmoid function which causes a steady-state error. Another approach, so-called as the higher-order sliding mode method, has been presented in reference [22] instead of the switching signal which can wipe out the chattering phenomenon. Furthermore, the tracking error convergence in finite-time is guaranteed by the higher-order sliding mode. Reference [23] implements the combination of two sliding surfaces, including the nonlinear terminal and PID sliding surface, to design the second-order fast TSMC. In the aforementioned paper, the uncertainty in the power coefficient model, and saturation in the electromagnetic torque has not been considered in the controller design procedure.

Another common problem in the control systems is the saturation nonlinearity in actuators which occurs because of the physical limitations and safety considerations. When the saturation occurs, the control input cannot be greater than its maximum and minimum limits, which not only does it reduce the performance of the system but can also cause instability in some cases. This issue has attracted a lot of attention in researchers which has led to the development of some methods to compensate for the input saturation. To compensate for the input saturation in a linear system the anti-windup compensator is an effective method. Reference [24] has presented the anti-windup PID control architecture for the linear systems. An investigation on the stability analysis for the problem of anti-windup design for a class of systems with discrete-time and time-varying, norm-bounded uncertainties and saturating actuators has been conducted by Zhang et al in [25]. When the saturation problem occurs in a nonlinear system, to design the actual input control law, usually there are two solutions available. The first solution is based on using the mean-value theorem to convert the input control to an affine form [26-28]. The second solution is based on defining an augmented error between the actual control input and the saturated control input and then designing an auxiliary dynamic variable to compensate for this error [29-32]. The previous researches studied the problem of input saturation in general systems and provided solutions to compensate for saturation. However, due to the safety considerations in Region 2 (the current limitation in electrical subsystem) and the physical limitations in Region 3 (limitation on the pitch angle because of limitation in servo actuator) in a wind turbine system, it is necessary for the saturation to be considered in the control input. Therefore, research on the design of an appropriate controller to compensate for the input saturation, especially for a wind turbine system seems to be a necessity. Reference [33] proposed an input-output feedback linearization nonlinear current controller to maximize the generated power in an Interior Permanent Magnet Synchronous Generator (IPMSG) driven by a wind turbine involved in magnetic saturation. In references [34, 35] to maximize the captured generated power in a variable speed wind turbine, the discrete sliding mode control is used. In these papers the saturation limitation is considered in the control input and to tackle this problem, in [34] the backstepping scheme is employed to construct an appropriate sliding surface that can guarantee the stability of the control system. In [35], the gains of the controller are designed using the Linear Matrix Inequality (LMI) so that the closed-loop

stability of the controller can be guaranteed in the presence of the input saturation. In this paper in order to have a linear system for easier controller design, it is assumed that the aerodynamic torque is a linear function. Reference [36] has developed a PI controller to control the current of a PMSG-based wind energy conversion system so that the presented controller has a good transient and asymptotically stability in the presence of the input saturation. References [33-36], have often either designed a linear controller only for the electrical subsystem of the wind turbine, or have assumed that the system is linear, and have designed a discrete-time sliding mode controller for the mechanical subsystem of the wind turbine.

Given that in the wind turbine both of the uncertainties and input saturation can occur, therefore considering the aerodynamic and mechanical model of the wind turbine with both uncertainties and input saturation is more general in practical applications. Moreover, to achieve a better precision and efficiency in the power generation, designing a controller with finite-time convergence for this model is very challenging. To the best of the authors' knowledge, according to the literature, the consideration of the uncertainties in the power coefficient and the dynamic model of the wind turbine as well as the consideration of the input saturation has not been studied. Based on the previous studies, the design of a high-precision robust controller with finite-time convergence has not been investigated yet. Therefore, designing a controller with a good performance against the model uncertainties and the input saturation, while the finite-time convergence is provided and the chattering and mechanical stresses problems are mitigated, can be very useful and efficient.

The main contribution of this paper is to propose a strategy, based on an adaptive fast TSMC in Region 2 of the operation area in the presence of the input saturation. At first, to reduce the mechanical stresses and to mitigate the chattering phenomenon, a second-order PI terminal sliding surface is considered. The integral term in the sliding surface can help to eliminate the steady-state error. Then, to ensure the finite-time convergence of the tracking error to zero, a nonlinear terminal surface is employed. Moreover, by adding a compensating variable to the tracking error, the second-order PI sliding surface is modified so that the input saturation can be compensated. The adaptation law for this dynamic compensating variable is designed so that the finite-time stability of the closed-loop system can be achieved. The simulation results show the superiority of the proposed scheme compared to the existing methods. The advantage of the proposed scheme is its ability to face the uncertainties in the model of the wind turbine as well as the input saturation which usually occurs in practice.

The outline of this paper is as follows. In Section 2, the wind turbine model is introduced. Section 3 presents the controller design procedure. The simulation results are given in Section 4. Finally, a conclusion for the proposed controller is presented in Section 5.

2. WIND TURBINE

As shown in Fig. 2, four subsystems can be considered to study the wind turbine characteristics. These subsystems are pitch servo subsystem, generator dynamic, aerodynamic subsystem and mechanical subsystem [37].

It is imperative to understand the principle of the wind turbine performance. According to Fig. 2, the wind speed causes the aerodynamic torque in the aerodynamic subsystem. To increase the efficiency of VSWT, some strategies such as flow control techniques [38, 39] can be utilized in this subsystem. As a result of the aerodynamic torque, the wind turbine blades start to rotate and this rotation leads to an angular velocity in the rotor side of the mechanical subsystem. The wind turbine and the generator are linked to each other via a gearbox thus, the generator shaft rotation speed, is higher than the rotor and the rotation of the generator leads to an electrical power in its output. To control the output electrical power, the electromagnetic torque and the pitch angle are used. To implement the maximum power point tracking strategy, the electromagnetic torque is used to capture the maximum power from the wind turbine in Region 2 and to fix the output power at its rated value in Region 3, the pitch servo subsystem is used. The servo subsystem increases the pitch angle by rotating the blades and as a result, the input aerodynamic torque is reduced and thus, the output power can be regulated at the nominal power.

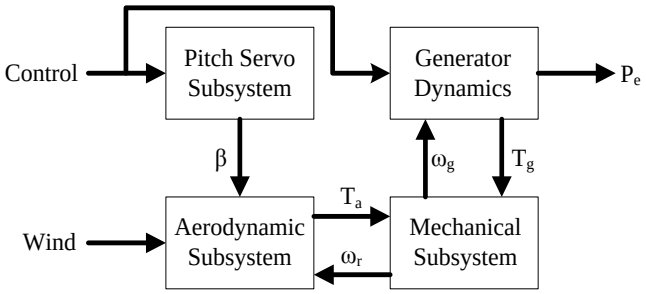

Figure 2. VSWT structure.

The wind turbine captures the wind power or the aerodynamic power. This power is a function of two parameters; the wind speed $V(t)$ and the power coefficient C_p, and the power coefficient itself depends on both the blade pitch angle β and also the tip speed ratio λ. To calculate the aerodynamic power, the following equation can be used [40]:

$$P_a = \frac{1}{2}\rho\pi R^2 C_p(\lambda,\beta)\, V^3(t) \tag{1}$$

In this equation, ρ represents the air density and R is the radius of the wind turbine rotor. In order to have a clear understanding of this equation, it is necessary to mention that the tip speed ratio λ is defined as:

$$\lambda = R\frac{\omega_r}{V} \tag{2}$$

where ω_r is the rotor speed. Therefore, the torque generated by the wind turbine is expressed as:

$$T_a = \frac{P_a}{\omega_r} = \frac{1}{2}\rho\pi R^3 \frac{C_p(\lambda,\beta)}{\lambda}\, V^2 \tag{3}$$

Due to the inherent uncertainties, the power coefficient is considered as follows:

$$C_p(\lambda,\beta) = \bar{C}_p(\lambda,\beta) + \Delta C_p(\lambda,\beta) \tag{4}$$

where $\bar{C}_p$ and $\Delta C_p(\lambda,\beta)$ are certain and uncertain terms of the power coefficient which are defined in Appendix A.

Note that, if the tip speed ratio has an optimum value, the power coefficient will be maximum that leads to maximum power extraction. To fix the tip speed ratio at its optimum value, the wind turbine speed should be controlled according to the input wind speed. To design an appropriate controller at first the dynamic model of the wind turbine should be described. As shown in Fig. 3, the model of the two-mass wind turbine is defined as follows [40]:

$$\begin{aligned} J_r\dot{\omega}_r &= T_a - T_{ls} - D_r\omega_r \\ J_g\dot{\omega}_g &= T_{hs} - T_e - D_g\omega_g \end{aligned} \tag{5}$$

where ω_r, ω_g and ω_{Ls} are the rotor, generator and low speed shaft angular velocities, respectively. T_e is the electromagnetic torque, T_{hs} is the high speed shaft torque and T_{ls} is the shaft torque in low speeds which is also known as the brake torque, and can be defined as:

$$T_{ls} = k_{ls}\left(\theta_r - \theta_{ls}\right) + D_{ls}\left(\omega_r - \omega_{Ls}\right) \tag{6}$$

where θ_{ls} and θ_r are the gearbox side and rotor side angular deviations, respectively.

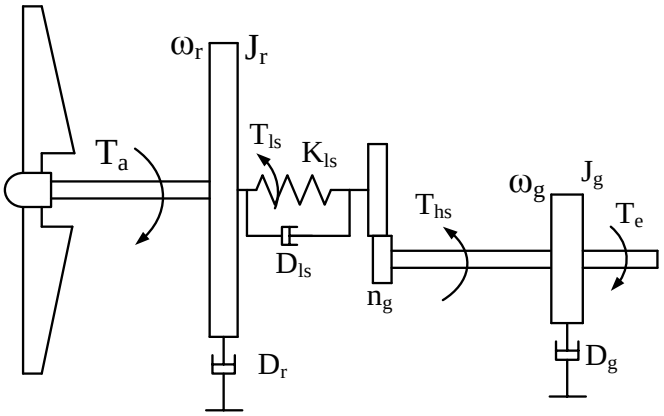

Figure 3. Two-mass wind turbine schematic.

Moreover, J_g, J_r are the generator and the rotor inertias, respectively. In addition, D_r, D_g and D_{ls} are the external damping coefficients of the rotor, the generator and the damping coefficient of the low speed shaft respectively. Moreover, n_g is the gearbox ratio which is defined as:

$$n_g = \frac{\omega_g}{\omega_{Ls}} = \frac{T_{Ls}}{T_{hs}} = \frac{\theta_g}{\theta_{Ls}} \tag{7}$$

Using (9), (10) and (11), it can be obtained that:

$$J_t\dot{\omega}_r = T_a - D_t\,\omega_r - T_g \tag{8}$$

where, $J_t = J_r + n_g^2 J_g$ is the turbine total inertia, $D_t = D_r + n_g^2 D_g$ is the total external damping of the turbine and $T_g = n_g T_e$ is the torque of the generator in the rotor side.

D_t and J_t are considered to be uncertain with unknown bounds based on the deviation with respect to the rated values, i.e.:

$$\begin{aligned} D_t &= \bar{D}_t + \Delta D_t, \left|\Delta D_t\right| \le \rho_{D_t} \\ J_t &= \bar{J}_t + \Delta J_t, \left|\Delta J_t\right| \le \rho_{J_t} \end{aligned} \tag{9}$$

where $\bar{J}_t$ and $\bar{D}_t$ are the rated values. Moreover, ρ_{J_t} and ρ_{D_t} are known constants with positive values.

Considering (3), (4) and (9), we can rewrite (8) as:

$$\dot{\omega}_r = \frac{1}{\bar{J}_t}[\bar{T}_a - \bar{D}_t\omega_r - n_g T_e + d(\lambda,\beta,V,\omega_r)] \tag{10}$$

where:

$$\begin{aligned} d(\lambda,\beta,V,\omega_r) &= [0.5\rho\pi R^3 \frac{\Delta C_P(\lambda,\beta)}{\lambda} V^2 - \Delta D_t\omega_r(t)] \\ &- \frac{\Delta J_t}{\bar{J}_t + \Delta J_t}[0.5\rho\pi R^3 \frac{C_P(\lambda,\beta)}{\lambda} V^2 - D_t\omega_r(t) - n_g T_e] \end{aligned} \tag{11}$$

And $\bar{T}_a$ is the rated aerodynamic torque and is defined as follows:

$$\bar{T}_a = 0.5\rho\pi R^3 \frac{\bar{C}_P(\lambda,\beta)}{\lambda} V^2 \tag{12}$$

The overall system parametric uncertainty is shown by the term, $d(\lambda, \beta, V, \omega_r)$ depending on (A.3) in Appendix A and (9). Inherent physical limitations of a practical wind turbine can cause the wind speed, the rotor speed and the blade pitch angle to have bounded ranges [41]. Thus, by considering (A.3) and (9), it can be assumed that there is a positive constant like $\bar{\delta} > 0$ so that the overall system parametric uncertainty can be bounded as:

$$\left|d(\lambda,\beta,V,\omega_r)\right| \le \bar{\delta}, \qquad \bar{\delta} > 0 \tag{13}$$

As it is known, in region 2 in wind energy systems, generator torque or electromagnetic torque is used as the control input to control the wind turbine output power. This torque has a relationship with the current of the generator. Therefore the control input cannot be very large because a large control input causes a great increase in the amount of the current, and this can damage the generator. So, it is necessary to have a limitation for generating the control input torque for safety purposes. In other words, the control input should be practically feasible and have a reasonable range. Therefore, due to physical limitations and safety purposes [35], in this paper, it is assumed that the generator torque has saturation limitation as follows.

$$T_e = \mathrm{sat}(u(t)) = \begin{cases} \mathrm{sign}(u(t)) \times T_{e_{max}}, & \left|u(t)\right| > T_{e_{max}} \\ u(t) & \left|u(t)\right| \le T_{e_{max}} \end{cases} \tag{14}$$

where $T_{e_{max}}$ is the maximum safe torque that can be applied to the system and $u(t)$ is the control input that needs to be designed.

The control objective is to maximize the extracted power from the wind which depends on the power coefficient, and the power coefficient itself depends on λ and β. Therefore, based on the power coefficient curve, as shown in Fig. 4, maximum of c_p can be computed based on λ_{opt} and β_{opt}. Furthermore, ω_{ropt} can be calculated based on the wind speed variations. The power coefficient curve is drawn based on (A.1) for various pitch angles and is illustrated in Fig. 4 and it can be seen that, the maximum value of c_p occurs at $\beta = 0$.

$$C_P\left(\lambda_{opt},\beta_{opt}\right)=C_{P_{max}} \tag{15}$$

$$\omega_{r_{opt}}=\frac{\lambda_{opt}V}{R} \tag{16}$$

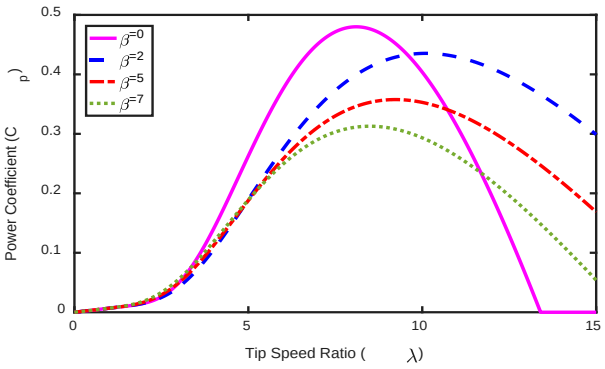

Figure 4. Power coefficient $C_P(\lambda,\beta)$ versus tip-speed ratio in different pitch angle.

Note that in this paper, like many other papers, the generator dynamic (Electrical Model) is not taken into account which can be considered as a future work to address the problem of input saturation by considering the generator dynamic. It is worth to note, in this paper, similar to many works in the field of the MPPT strategy for the wind turbine, the speed control is investigated and direct power control is not considered. So according to the wind speed in region 2 and power coefficient curve (according to (A.1)), to achieve the maximum power, we should apply a generator torque to the wind turbine (according to (5)) that can regulate the turbine speed at its optimum value corresponding to the wind speed at each instant. Therefore, the power coefficient will has its maximum value, and the maximum power can be extracted from the input wind power. It is worth noting that in this strategy, the wind power is converted to the generator speed and there is no direct conversion between the generator torque and the wind power because the generator torque is determined by the controller.

Before presenting the controller design procedure, the following Lemma needs to be introduced. This Lemma is defined to prove the finite-time stability of the closed-loop system after applying the proposed controller.

Lemma 2.1 [42]: For any positive-definite function $V(t)$ which fulfills a differential inequality as:

$$\dot{V}(t)+\alpha\, V(t)+\beta\, V^{\ell}(t)\le 0 \tag{17}$$

where α and β are two positive coefficients, and ℓ is a fraction of two odd positive numbers with $1>\ell>0$, for the certain time t_0, note that the aforementioned function V(t), converges to zero in the finite-time t_r as:

$$t_r\le t_0+\frac{1}{\alpha(1-\ell)}\ln\left(\frac{\alpha\, V^{1-\ell}(t_0)+\beta}{\beta}\right) \tag{18}$$

3. CONTROLLER DESIGN

In this section, an adaptive second-order fast TSMC (SOFTSMC) is designed for harvesting the maximum power in a wind turbine (WT) system subjected to input control limitation. This method is performed in two main steps. First, the sliding surface is defined and in the second step, by considering the sliding dynamics, a controller is designed such that the tracking error will converge to zero in finite-time. In the first step, a fast terminal sliding surface is considered as below that can ensure that the sliding surface converges to zero in finite-time:

$$\sigma(t)=k_{1\sigma}\, s(t)^{\frac{p}{q}}+k_{2\sigma}\, s(t)+k_{3\sigma}\,\dot{s}(t) \tag{19}$$

Note that $k_{1\sigma}$ and k_{3s} are positive design parameters. In the second step, to decrease the mechanical stresses and mitigate the chattering and also to eliminate the steady state error, a second-order integral terminal sliding dynamic equation is considered as:

$$\dot{s}(t)+\gamma\, s(t)=k_p\, z(t))+k_I\int_0^t(k_{1I}\, z(\tau)^{\frac{p}{q}}+k_{2I}\, z(\tau))\,d\tau \tag{20}$$

where $z(t)=e(t)+\eta(t)$. $e(t)$ and $\eta(t)$ are tracking error and auxiliary dynamic variables, respectively. Note that $\eta(t)$ is considered to compensate for the effect of input saturation. To achieve the finite-time convergence for the tracking error, the term $z(\tau)^{\frac{p}{q}}$ has been added into the sliding surface, where γ, k_p, k_I, k_{1I} and k_{2I} are positive design parameters. In addition, p and q are arbitrary positive odd constants so that the following inequality holds:

$$\frac{1}{2}<\frac{p}{q}<1 \tag{21}$$

The speed tracking error is defined as:

$$e(t)=\omega_r(t)-\omega_d(t)=\omega_r(t)-\omega_{r_{opt}}(t) \tag{22}$$

where $\omega_{r_{opt}}$ is the required rotor speed to achieve the maximum power in the wind turbine system.

As it is known, the conventional sliding surface is a combination of the error and the derivative of the error; however, by adding the integral of error and constructing a PID sliding surface, the steady-state error converges to zero. In [23], a PID second-order sliding surface has been used. In the proposed method, by adding the derivative of the sliding surface to the right hand side of the conventional PID sliding surface, not only the advantages of a conventional PID sliding surface are provided, but also the chattering is reduced. In this paper, a PI second-order sliding surface is employed for two reasons; first, the derivative of the tracking error in the aforementioned PID second-order sliding surface increases the order of the system and secondly, to compute the actual input control, the time derivative of the aerodynamic torque and the second order time derivative of the optimal rotor speed are needed.

In this paper, on the contrary to [23], in both aerodynamic (C_p) and mechanical models of the two-mass wind turbine, it is assumed that the model parameters are uncertain. Moreover, in this paper, the input saturation is also taken into account. To solve the saturation problem, a compensating dynamic term is added to the tracking error, and also the second-order

PI sliding surface is constructed based on this compensating variable. Then the adaptation law of this compensating dynamic term is designed so that the finite-time convergence of the closed-loop system can be ensured. Furthermore, the nonlinear integral term of the error, which was added to the second-order PI sliding surface, can ensure that the tracking error converges to zero in finite-time, while in [23] the tracking error is asymptotically stable and converges to zero in finite-time.

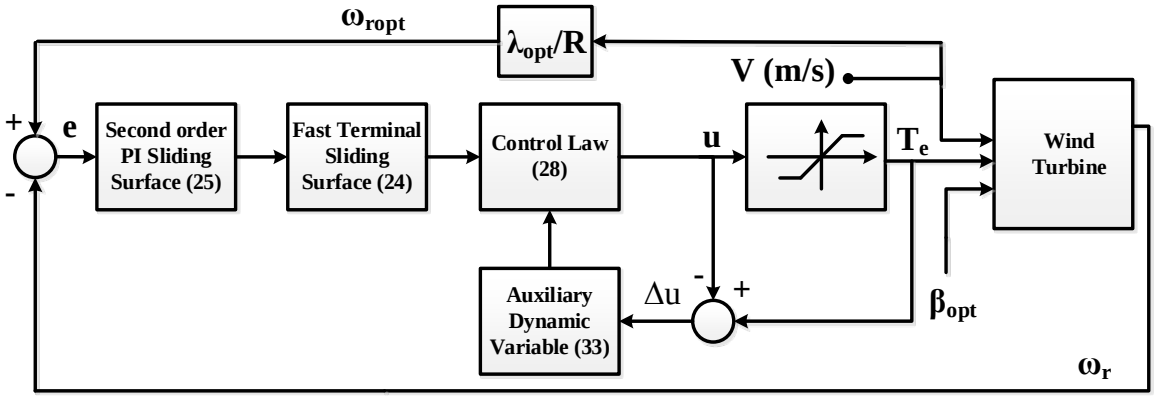

Figure 5. The closed-loop block diagram of the proposed controller.

Theorem 1. In the dynamic model of the wind turbine (10), by applying the following control input and also by selecting the control parameters such that $b_4 > \frac{\alpha_1}{\alpha_3}\overline{\Delta u}$ and $b_2 > \alpha_2 \bar{\delta}$ hold, where $\overline{\Delta u}$ is the upper bound of $\Delta u = T_e - u$, then the overall system will be stable and the tracking error will converge to zero in finite-time:

$$u = -\frac{1}{\alpha_1}[-f - b_1\,\sigma(t) - b_2\,\mathrm{sign}(\sigma(t))) + \alpha_3\,b_3\,\eta(t) + \alpha_3\,b_4\,\mathrm{sign}(\eta(t))] \quad (23)$$

where:

$$f = \varphi(-\gamma s(t) + w) + k_{3\sigma}\,k_p\left[\frac{1}{\bar{J}_t}\left[\bar{T}_a - \bar{D}_t\omega_r\right] - \dot{\omega}_{r_{opt}}(t)\right] + k_{3\sigma}\left[k_{I_1} z(t)^{\frac{p}{q}} + \left(k_{I_2} + \frac{k_p}{k_{3\sigma}}\varphi\right) z(t)\right] \quad (24)$$

$$\varphi = k_{1\sigma}\frac{p}{q}s(t)^{\frac{p}{q}-1} + k_{2\sigma} - \gamma k_{3\sigma} \quad (25)$$

$$w = k_I \int_0^t (k_{1I}\, z(\tau)^{\frac{p}{q}} + k_{2I}\, z(\tau))\, d\tau \quad (26)$$

$$\alpha_1 = n_g k_{3\sigma}\frac{k_p}{\bar{J}_t},\ \alpha_2 = k_{3\sigma}\frac{k_p}{\bar{J}_t}, \alpha_3 = k_{3\sigma}k_p \quad (27)$$

Moreover, the adaptation law for the dynamic variable $\eta(t)$ which is defined to compensate for the input saturation is designed as:

$$\dot{\eta}(t) = -b_3\,\eta(t) + \frac{\alpha_1}{\alpha_3}\Delta u - b_4\,\mathrm{sign}(\eta(t)) \quad (28)$$

where b_3 and b_4 are positive arbitrary constants. Note that $-b_4\,\mathrm{sign}(\eta(t))$ is added to achieve the finite-time convergence in the proposed adaptive controller in the presence of the input saturation.

Proof. See Appendix B.

The augmented dynamic variable is designed to compensate for the input saturation problem. For a normal case, when the input saturation does not occur, this augmented variable is stable and converges to zero in the finite-time and when the saturation occurs, based on (28), the term Δu causes that $\eta \neq 0$, and therefore, according to (23), this variable helps the controller for the input saturation compensation.

The closed-loop block diagram of the proposed controller is shown in Fig. 5.

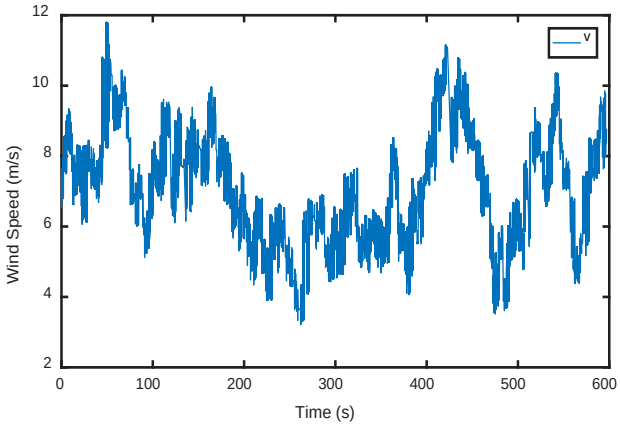

Figure 6. Wind speed profile.

4. SIMULATIONS

To demonstrate the performance of the proposed controller against the parameter uncertainties and the input saturation, various simulations have been employed. The performance of the proposed controller is compared with some of the existing methods for two cases. In Case 1, the model uncertainties and the input saturation are not considered, while in Case 2, 60 % of the parameter uncertainty and the input saturation are considered. The wind speed in the wind turbine system is considered as shown in Fig. 6. Simulations are performed for 600 seconds, the mean value of the wind speed is 7.5 m/s and the turbulence intensity is 18 %. To have smooth signals, the optimal rotor speed after passing a low-pass filter is applied to the controller. By fitting Eq. (A.1) with the values of C_p for

the NREL 5-MW wind turbine, the rated values for $\bar{c}_i$, i=1 … 5 are as below [23]:

$$\bar{c}_1 = 0.5176,\ \bar{c}_2 = 116,\ \bar{c}_3 = 0.4,\ \bar{c}_4 = 5,\ \bar{c}_5 = 21,\ \bar{c}_6 = 0.0068 \quad (29)$$

The wind turbine parameters, used in these simulations, are selected the same as reported in [23] which are listed in Table 1.

In this paper, the MATLAB software is used to simulate the wind turbine model and the designed controller. The model of the wind turbine which is described in (5) and (6) is used and these differential equations have been implemented in Simulink environment. The ode45 solver has been employed to solve the differential equations. It is worth noting that the wind turbine model in (5) and (6) has been utilized in many of the references related to the control of the wind turbine. The details about this model and its validation can be found in [40, 43, 44] and references therein.

The proposed method is compared with conventional first order SMC (FOSMC) and two strategies that have been proposed in [23], named PID second-order SMC (SOSMC) and second-order fast TSMC (SOFTSMC).

Table 1. Wind turbine model parameters.

R	21.65	m
ρ	1.308	Kg/m^3
J_g	34.4	$Kg.m^2$
J_r	3.25×10^5	$Kg.m^2$
D_r	27.36	N.m/rad/s
D_g	0.2	N.m/rad/s
K_{1s}	9.5×10^3	N.m/rad
D_{1s}	2.691×10^5	N.m/rad/s
P_{enom}	600×10^5	W
T_{emax}	3×10^3	N.m
β_{opt}	0	deg
λ_{opt}	8.1	-
n_g	43.165	-

The control law for the FOSMC is designed as:

$$\begin{cases} s = \dot{e} + k\,e \\ \dot{u} = \dfrac{\bar{J}_t}{n_g}\left[\dfrac{1}{\bar{J}_t}(\dot{\bar{T}}_a - \bar{D}_t\,\dot{\omega}_r - \ddot{\omega}_{ropt} + k\dot{e}) + k_{sw}\,\mathrm{sign}(s)\right] \end{cases} \quad (30)$$

The control parameters for this controller are chosen as:

k = 2 and k_{sw} = 0.1.

The control input for the SOSMC and the SOFTSMC are given in (31) and (32), respectively.

$$\begin{aligned} & s = \dot{e} + k\,e \\ & \dot{s} + \gamma s = k_p\,e + k_I \int_0^t e(\tau)\,d\tau + k_D\,\dot{e} \\ & \dot{u} = \frac{\bar{J}_t}{n_g(k_D - \gamma)}[(k\gamma - k_P)\,\dot{e} - k_I\,e + (\gamma - k_D)\,\ddot{\omega}_{ropt} \\ & \quad - \frac{(\gamma - k_D)}{\bar{J}_t}\dot{\bar{T}}_a + \frac{(\gamma - k_D)\bar{D}_t}{\bar{J}_t}\dot{\omega}_r)] - \beta_1 s - \beta_2\,\mathrm{sign}(s) \end{aligned} \quad (31)$$

where $k = 100,\ \gamma = 6, k_p = 5, k_I = 0.1, k_D = 50, \beta_1 = 0.1$ and $\beta_2 = 0.1$.

$$\begin{aligned} & s = \dot{e} + k\,e \\ & \dot{s} + \gamma s = k_p\,e + k_I \int_0^t e(\tau)\,d\tau + k_D\,\dot{e} \\ & \sigma = s^{\frac{p}{q}} + \dot{s} + s \\ & \vartheta = \frac{p}{q} s^{\frac{p}{q}-1} + 1 - \gamma \\ & \dot{u} = \frac{\bar{J}_t}{n_g(\vartheta + k_D)}[-(\vartheta k + k_P)\,\dot{e} - k_I\,e + (\vartheta + k_D)\,\ddot{\omega}_{ropt} \\ & \quad + \frac{(\vartheta + k_D)}{\bar{J}_t}(\dot{\bar{T}}_a - \bar{D}_t\dot{\omega}_r) - k_{sw1}\,s - k_{sw2}\,\mathrm{sign}(s)] \end{aligned} \quad (32)$$

where

$$k = 100,\ \gamma = 6, k_p = 5, k_I = 0.1,$$
$$k_D = 50, k_{sw1} = 0.1, k_{sw2} = 0.01, p = 17$$

and $q = 19$.

Finally, based on (23)-(28), parameters of the proposed controller are selected as:

$$\gamma = 1, k_p = 1, k_I = 1, k_{1I} = 1, k_{2I} = 1, k_{1\sigma} = 1, k_{2\sigma} = 1,$$
$$k_{3\sigma} = 1\times10^3, b_1 = 20, b_2 = 0.1, b3 = 1, b_4 = 0.1, p = 17$$

and $q = 19$.

As previously mentioned, the simulations are performed for two cases. Case 1 is without the uncertainty and the input saturation, while in Case 2 both of the uncertainty and the input saturation are considered.

Fig. 7 to Fig. 12 illustrates the comparative results of Case 1 and Fig. 7, illustrates the rotor speed. It is obvious that the proposed controller has a better tracking performance compared to the existing methods. The proposed controller not only has less steady state error but also has a better dynamic performance. The generator speed for 4 controllers is shown in Fig. 8. The electromagnetic torque that is used as a control law is demonstrated in Fig. 9. As shown in the control law of the FOSMC, the chattering phenomenon has appeared. This can cause serious damage to the wind turbine and the rest of the controllers have no chattering. Low-speed shaft torque is demonstrated in Fig. 10 and according to this figure the Low-speed shaft in the FOSMC controller is involved in chattering problem that increases the mechanical stress on wind turbine. While, this problem does not appear in the proposed controller and also in the SOSMC and the SOFTSMC controllers. The electrical power P_e that is harvested from the wind turbine is depicted in Fig. 11 and the maximum power is captured by the proposed controller, and

as it can be seen from Figure 11, electrical power has many deviations due to the chattering phenomenon. The rotor speed tracking error is shown in Fig. 12 and it can be seen that the tracking error of the proposed controller is less than the others.

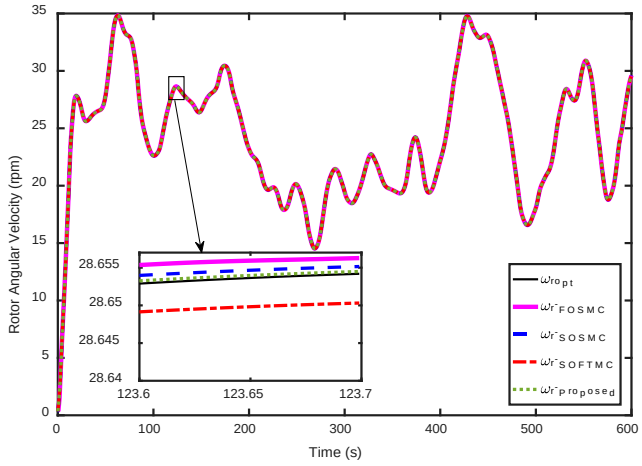

Figure 7. Rotor speed for Case 1.

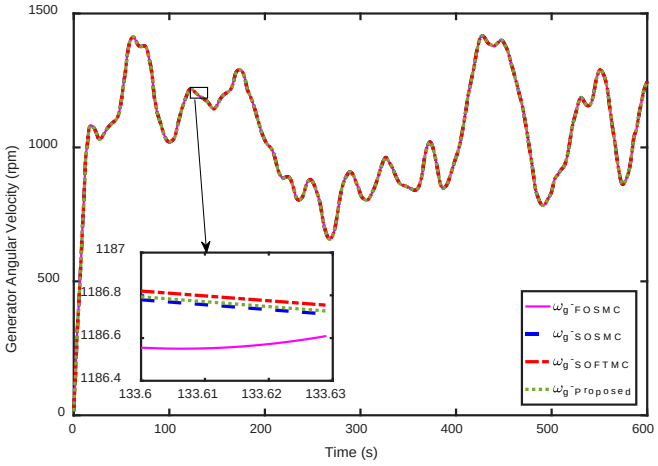

Figure 8. Generator speed for Case 1.

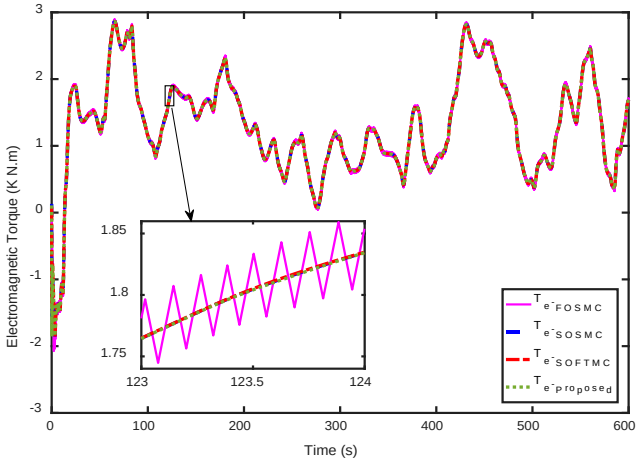

Figure 9. Electromagnetic torque (control input) for Case 1.

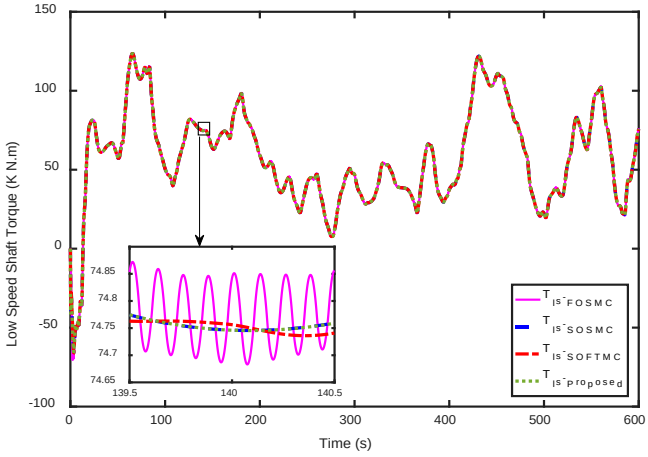

Figure 10. Low-speed shaft torque for Case 1.

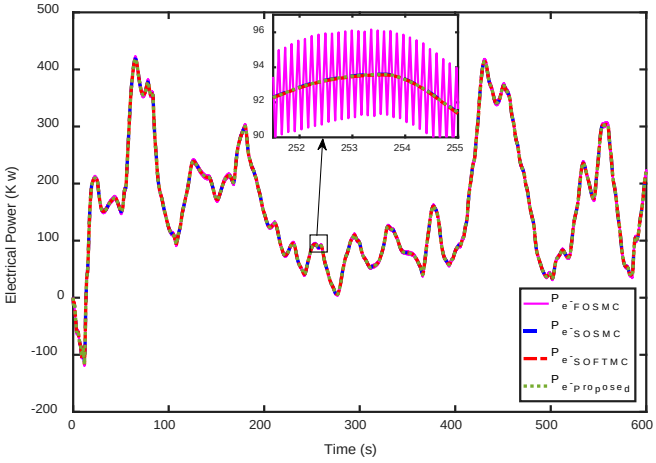

Figure 11. Electrical power for Case 1.

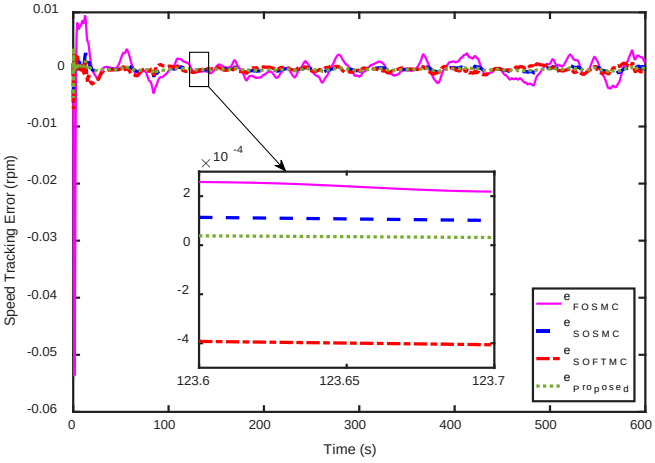

Figure 12. Rotor speed tracking error for Case 1.

As mentioned earlier, given that the existing controllers are not designed for a wind turbine model involved in both uncertainties in the aerodynamic and the mechanical model as well as input saturation in the control law, therefore, due to taking into account the aforementioned uncertainties in the proposed controller design procedure as well as the design of an auxiliary dynamic variable to compensate for the input saturation, it is expected that the proposed controller has a better performance than the existing controllers in facing the aforementioned problems. Therefore, in the second case, the superiority of the proposed controller is more distinct than the aforesaid controllers. Fig.13 to Fig.18, show the results of applying above-mentioned controller to the wind turbine, for Case 2. Fig. 13 shows the rotor speed in the presence of model parameters uncertainties and input saturation. It is obvious that the proposed controller shows a very promising

performance and tracks the optimal rotor speed very faster than the other controllers which have been mentioned above. In Fig. 14, the generator speed for four controllers is shown. The electromagnetic torque which is the control input is shown in Fig. 15 for various controllers. As it is shown, the FOSMC is involved in the chattering. Fig. 16 shows the low-speed shaft torque for 4 different controllers and as in the previous case, the mechanical stresses caused by the chattering phenomenon which appeared in the Low-speed shaft torque, are reduced in the proposed controller. The extracted electric power is depicted in Fig. 17. Moreover, Fig. 18 shows the rotor speed tracking error. In this figure, the tracking error for the proposed controller is less than the other aforementioned controllers and the superiority of the proposed controller in Case 2 is more evident than Case 1. Therefore, the proposed controller not only has good steady-state properties, but also has better transient-state properties than the existing controllers, in the presence of input uncertainties and saturation.

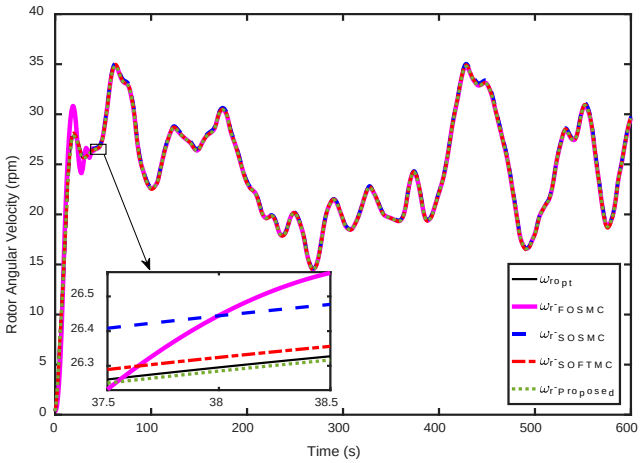

Figure 13. Rotor speed for Case 2.

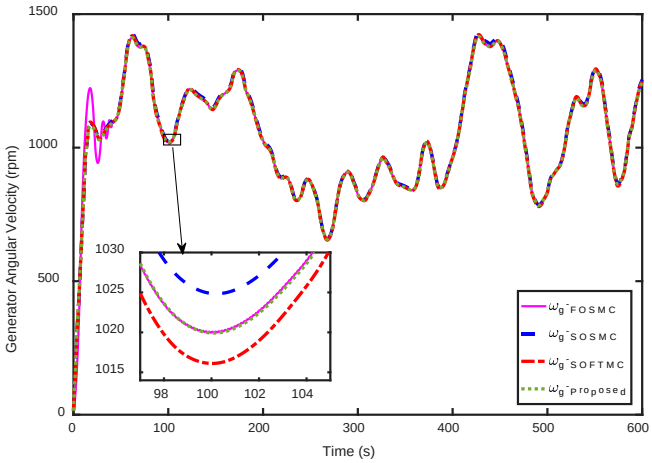

Figure 14. Generator speed for Case 2.

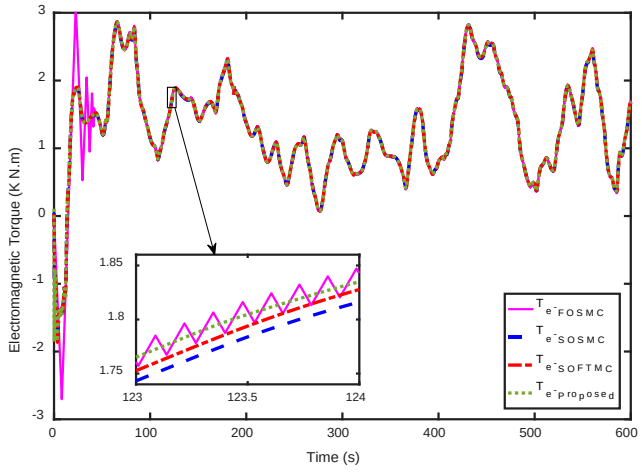

Figure 15. Electromagnetic torque (control input) for Case 2.

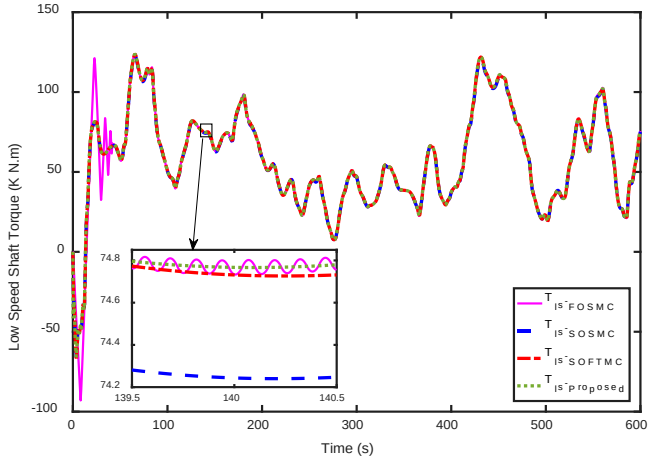

Figure 16. Low-speed shaft torque for Case 2.

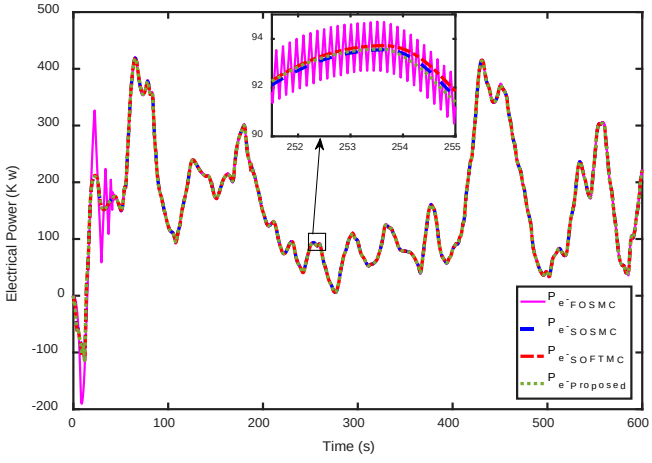

Figure 17. Electrical power for Case 2.

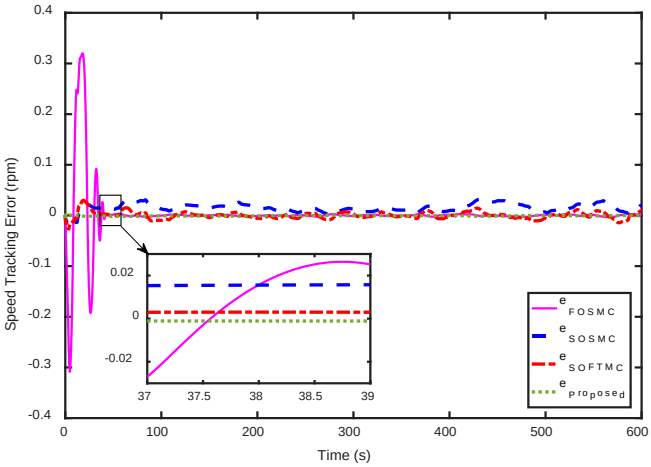

Figure 18. Rotor speed tracking error for Case 2.

Finally, performance indices, i.e., integral of the absolute error (IAE) and the integral of the square error (ISE) and the integral of the time multiply absolute error (ITAE) have been calculated for these controllers as presented in the Table 2. It can be seen that the proposed controller in all three indices is superior to the other three controllers and it should be noted that in Case 2 the performance indices for the proposed controller are smaller than the others. Thus, the results of the proposed scheme are very promising and satisfactory, even when input saturation and uncertainties are considered in the wind turbine system. However, other existing controllers have less performance compared to this controller.

Table 2. Performance indices comparison for different controllers.

	Case 1			Case 2		
Controller	IAE	ISE	ITAE	IAE	ISE	ITAE
FOSMC	0.8639	0.0058	228.44	6.9424	1.4379	327.4257
SOSMC	0.1636	9.3830e-05	47.5803	9.4274	0.1761	2.7936e+03
SOFTSMC	0.2322	1.7708e-04	65.8714	3.1197	0.0293	870.6477
Proposed	0.0830	2.7154e-05	23.8139	0.3886	3.8845e-04	95.1887

The aforementioned performance indices are computed using the criteria described by (34).

$$\begin{cases} IAE = \int \left| e(t) \right| dt \\ ISE = \int e^2(t) dt \\ ITAE = \int t \left| e(t) \right| dt \end{cases} \quad (33)$$

Table 3 is provided to evaluate the performance of the proposed controller and conventional existing controllers using the aerodynamic and electrical efficiency. Aerodynamic efficiency η_{aero} and electrical efficiency η_{elec} can be calculated using the following equations.

$$\eta_{aero}(\%) = \frac{\int_{t_i}^{t_f} P_a(t)\,dt}{\int_{t_i}^{t_f} P_{aopt}(t)\,dt} \times 100, \qquad \eta_{aero}(\%) = \frac{\int_{t_i}^{t_f} P_{elec}(t)\,dt}{\int_{t_i}^{t_f} P_{aopt}(t)\,dt} \times 100 \quad (34)$$

where $P_{aopt} = 0.5\rho\pi R^2 C_{pmax} V^3$ is the optimal aerodynamic power, P_{elec} is the electrical power, t_i is the initial simulation time and t_f is the final simulation time.

Table 3. Efficiency comparison for different controllers.

	Case 1		Case 2	
Controller	η_{aero}	η_{elec}	η_{aero}	η_{elec}
FOSMC	90.22	88.72	85.233	82.088
SOSMC	94.357	92.04	89.427	86.781
SOFTSMC	95.82	93.49	90.119	87.521
Proposed	96.513	95.65	92.388	90.087

According to the Table 3, the FOSMC controller has the least efficiency in terms of the aerodynamics and electricity. However, the efficiency of the SOSMC controller and the SOFTSMC controller is almost the same, and the SOFTSMC controller is more efficient than the SOSMC controller. It is obvious that the proposed controller has the best efficiency rather than the existing controllers and by using this proposed controller the aerodynamic and electrical efficiency has been increased about 3 % in the Case 2.

5. CONCLUSIONS

The maximum power extraction from the wind in a wind turbine is difficult especially when there are model uncertainties in the system and the task becomes more challenging when the control input has saturation in its amplitude. Sliding mode controller is a suitable control method to deal with these inevitable uncertainties. But the conventional SMC causes the chattering problem that increases the mechanical stress on the wind turbine. By designing a second-order sliding mode controller the chattering problem can be avoided. However, to achieve high efficiency and precision in capturing the power, the terminal sliding mode control can provide satisfactory results thanks to its finite-time convergence properties. When the control input is constrained, the finite-time convergence of the control that is designed for normal condition i.e. without the input constraint cannot be guaranteed. Therefore, designing a controller that has a high precision and efficiency in the presence of model uncertainties and input saturation, as well as finite-time convergence properties, is practically effective. Given that in the previous works, the problem of finite-time controller design in the presence of the both uncertainties in the aerodynamic and the mechanical model, as well as input saturation in the control law, is not considered. However, in this paper, unlike the previous works, by considering the uncertainties and input saturation simultaneously, a finite-time convergent controller has been investigated. In this paper, to capture the maximum power, low mechanical stress, and to improve the tracking performance of the wind turbine system with parametric uncertainties in model and saturation in input, an adaptive second-order fast ITSMC has been proposed. It has been proven that the designed controller can achieve the zero tracking error in the finite-time even when the input saturation and the uncertainties of the system parameters are present. The augmented dynamic variable that was used to compensate for the input saturation was modified so that the finite-time convergence is ensured. Numerical Simulations are performed for two cases, without the uncertainty and the input saturation and with the uncertainty and the input saturation. In both cases, the proposed controller yielded satisfactory results and in the second case, the superiority of the proposed controller has been more evident than the others. As presented in Table 3, using the proposed controller in Case 2, the aerodynamic and electrical efficiency has been increased by almost 3 % compared to the SOFTSMC controller which is

the most efficient among the existing controllers. Meanwhile, in any kind of controller, the overshoot problem may occur, which can cause an illegal speed in the wind turbine, so in some applications, it is necessary that it should be guaranteed that the speed of the wind turbine can be constrained in a prescribed bound. Furthermore, in practical systems, input delay, sensors and actuator faults occur where may lead to damage to the wind turbine. Apart from that, because of the inherent model uncertainties in the wind turbine, designing a disturbance observer can reduce the input electromagnetic torque and the low-speed shaft torque significantly. Since in the existing controller these limitations are not considered, then the future works can concern the controller design in the presence of state constraint, the robust fault-tolerant control and input delay and disturbance observer design for the wind turbine system.

6. ACKNOWLEDGEMENT

The authors would like to acknowledge the support of the Babol Noshirvani University of Technology through Grant No. BNU/370632/2020.

NOMENCLATURE

C_p	Power coefficient
β	Blade pitch angle
λ	Tip speed ratio
ρ	Air density
R	Wind turbine rotor radius
ω_r	Rotor angular velocity
ω_g	Generator speed
ω_{Ls}	Low speed shaft angular velocity
T_e	Electromagnetic torque
T_{hs}	High speed shaft torque
T_{1s}	Low speed shaft torque
θ_{1s}	Gearbox angular deviation
θ_r	Rotor angular deviation
J_g	Generator inertia
J_r	Rotor inertia
D_r	Rotor damping coefficient
D_g	Generator damping coefficient
D_{1s}	Low speed shaft damping coefficient
n_g	Gearbox ratio
J_t	Total inertia of the turbine
D_t	Total external damping of the turbine
T_g	Generator torque in the rotor side

Abbreviations

VSWT	Variable speed wind turbine
MPPT	Maximum power point tracking
PI	Proportional-integral
PID	Proportional-integral-derivative
LQ	Linear-quadratic
LQG	Linear–quadratic–Gaussian
SMC	Sliding mode control
ISMC	Integral sliding mode control
TSMC	Terminal sliding mode control
ITSMC	Integral terminal sliding mode control
NTSMC	Non-singular terminal sliding mode control
FOSMC	First order sliding mode control
SOSMC	Second order sliding mode control
SOFTSMC	Second-order fast terminal sliding mode control
WT	Wind turbine
IAE	Integral of absolute error
ISE	Integral of square error
ITAE	Integral of time multiply absolute error
DFIG	Doubly-fed induction generator
NN	Neural network
RBF	Radial-basis-function
IPMSG	Interior permanent magnet synchronous generator
LMI	Linear matrix inequality

APPENDICES

Appendix A. Power coefficient properties

The power coefficient of the wind turbine C_p can be expressed as follows:

$$C_p(\lambda,\beta) = c_1\left(\frac{c_2}{\lambda_i} - c_3\beta - c_4\right)\exp\left(\frac{-c_5}{\lambda_i}\right) + c_6\lambda$$
$$\frac{1}{\lambda_i} = \frac{1}{\lambda + 0.08\beta} - \frac{0.035}{\beta^3 + 1} \quad (A.1)$$

The coefficients c_i, i= 1…5 are based on two parameters. The first parameter is the shape of the wind turbine blades and the second parameter is the aerodynamic performance of the blades. These coefficients are considered to be uncertain as:

$$c_i = \bar{c}_i + \Delta c_i \quad i = 1,2,...,5 \quad (A.2)$$

It is also assumed that the uncertainties $\Delta c_i\ i = 1,2,...,5$ are bounded with unknown bounds as follows:

$$|\Delta c_i| \le \rho_{c_i} \quad (A.3)$$

where ρ_{c_i} are the unknown positive constants.

Thus, the following functions can be defined:

$$h_1(\lambda,\beta) = \left(\frac{\bar{c}_2}{\lambda_i} - \bar{c}_3\beta - \bar{c}_4\right)$$
$$h_2(\lambda,\beta) = c_1\left(\frac{\Delta c_2}{\lambda_i} - \Delta c_3\beta - \Delta c_4\right) + \Delta c_1\, h_1(\lambda,\beta)$$
$$\bar{C}_p(\lambda,\beta) = \bar{c}_1 h_1(\lambda,\beta)\exp\left(\frac{\bar{c}_5}{\lambda_i}\right) + \bar{c}_6\lambda$$
$$\Delta C_p(\lambda,\beta) = \left[\bar{c}_1\, h_1(\lambda,\beta) + h_2(\lambda,\beta)\right] \times\left[\exp\left(\frac{\bar{c}_5}{\lambda_i}\right)\left(\exp\left(\frac{\Delta c_5}{\lambda_i}\right) - 1\right)\right] + h_2(\lambda,\beta)\exp\left(\frac{\bar{c}_5}{\lambda_i}\right) + \Delta c_6\lambda \quad (A.4)$$

Therefore, the power coefficient can be rewritten as:

$$C_p(\lambda,\beta) = \bar{C}_P(\lambda,\beta) + \Delta C_p(\lambda,\beta) \tag{A.5}$$

Appendix B. Proof of theorem 1

To analyze the stability and the finite-time convergence of the proposed controller, consider the following Lyapunov function:

$$V = \frac{1}{2}\sigma(t)^2 \tag{B.1}$$

Differentiating V with respect to time yields:

$$\dot{V} = \sigma(t)\dot{\sigma}(t) \tag{B.2}$$

Using (19), we have:

$$\begin{aligned}\dot{\sigma}(t) &= \frac{k_{1\sigma}\, p}{q} s(t)^{\frac{p}{q}-1}\dot{s}(t) + k_{2\sigma}\dot{s}(t) + k_{3\sigma}\ddot{s}(t)\\ &= \left(\frac{k_{1\sigma}\, p}{q} s(t)^{\frac{p}{q}-1} + k_{2\sigma}\right)\dot{s}(t) + k_{3\sigma}\ddot{s}(t)\end{aligned} \tag{B.3}$$

Moreover, from (20), (B.4) is obtained as:

$$\ddot{s}(t) = -\gamma\dot{s}(t) + k_p\dot{z}(t) + k_I\left(k_{1I} z(t)^{\frac{p}{q}} + k_{2I} z(t)\right) \tag{B.4}$$

For simplification, the terms $k_{I_1} = k_I k_{1I}$ and $k_{I_2} = k_I k_{2I}$ are defined. By substituting (B.4) into (B.3), (B.5) is obtained as:

$$\begin{aligned}\dot{\sigma}(t) = &\left(\frac{k_{1\sigma} p}{q} s(t)^{\frac{p}{q}-1} + k_{2\sigma} - k_{3\sigma}\gamma\right)\dot{s}(t) + \left(k_p\dot{z}(t)\right.\\ &\left. + k_{I_1} z(t)^{\frac{p}{q}} + k_{I_2} z(t)\right) k_{3\sigma}\end{aligned} \tag{B.5}$$

On the other hand, the time derivative of $z(t)$ can be calculated as follows:

$$\begin{aligned}\dot{z}(t) &= \dot{\omega}_r(t) - \dot{\omega}_{r_{opt}}(t) + \dot{\eta}(t)\\ &= \frac{1}{\bar{J}_t}\left[\bar{T}_a - \bar{D}_t\omega_r - n_g T_e + d(\lambda,\beta,V,\omega_r)\right] - \dot{\omega}_{r_{opt}}(t) + \dot{\eta}(t)\end{aligned} \tag{B.6}$$

Replacing (20) into (B.5), gives:

$$\begin{aligned}\dot{\sigma}(t) = &\left(k_{1\sigma}\frac{p}{q} s(t)^{\frac{p}{q}-1} + k_{2\sigma} - \gamma k_{3\sigma}\right)\times\left(-\gamma s(t) + k_p z(t)\right.\\ &\left. + k_I\left(\int_0^t \left(k_{1I} z(\tau)^{\frac{p}{q}} + k_{2I} z(\tau)\right) d\tau\right)\right.\\ &\left. + k_{3\sigma}\left(k_p\dot{z}(t) + k_{I_1} z(t)^{\frac{p}{q}} + k_{I_2} z(t)\right)\right.\end{aligned} \tag{B.7}$$

By substituting (25), (26) and (B.6) into (B.7), it can be obtained that:

$$\begin{aligned}&\dot{\sigma}(t) = \varphi(-\gamma s(t) + w)\\ &+ k_{3\sigma}k_p\left[\frac{1}{\bar{J}_t}\left[\bar{T}_a - \bar{D}_t\omega_r - n_g T_e + d(\lambda,\beta,V,\omega_r)\right]\right]\\ &- k_{3\sigma}k_p\left[\dot{\omega}_{r_{opt}}(t) + \dot{\eta}(t)\right]\\ &+ k_{3\sigma}\left[k_{I_1} z(t)^{\frac{p}{q}} + \left(k_{I_2} + \frac{k_p}{k_{3\sigma}}\varphi\right) z(t)\right]\\ &= \varphi(-\gamma s(t) + w) + k_{3\sigma}k_p\left[\frac{1}{\bar{J}_t}\left[\bar{T}_a - \bar{D}_t\omega_r\right] - \dot{\omega}_{r_{opt}}(t)\right]\\ &+ k_{3\sigma}\left[k_{I_1} z(t)^{\frac{p}{q}} + \left(k_{I_2} + \frac{k_p}{k_{3\sigma}}\varphi\right) z(t)\right] - \left(n_g k_{3\sigma}\frac{k_p}{\bar{J}_t}\right) T_e\\ &+ k_{3\sigma}k_p\dot{\eta}(t) + \frac{k_{3\sigma}k_p}{\bar{J}_t} d(\lambda,\beta,V,\omega_r)\end{aligned} \tag{B.8}$$

Using (24) and (27), (B.8) becomes:

$$\begin{aligned}\dot{\sigma}(t) &= f - \left(n_g k_{3\sigma}\frac{k_p}{\bar{J}_t}\right) T_e + \frac{k_{3\sigma}k_p}{\bar{J}_t} d(\lambda,\beta,V,\omega_r) + k_{3\sigma}k_p\dot{\eta}(t)\\ &= f - \alpha_1 T_e + \alpha_2\, d(\lambda,\beta,V,\omega_r) + \alpha_3\,\dot{\eta}(t)\\ &= f - \alpha_1 u - \alpha_1\Delta u + \alpha_2\, d(\lambda,\beta,V,\omega_r) + \alpha_3\,\dot{\eta}(t)\end{aligned} \tag{B.9}$$

By replacing (23), (30) and (B.9) into (B.1), (B.2) can be written as:

$$\dot{V} = \sigma(t)\left(-b_1\sigma(t) - b_2\,\mathrm{sign}(\sigma(t)) + \alpha_2\, d(\lambda,\beta,V,\omega_r)\right) \tag{B.10}$$

Using (13), the following inequality is derived:

$$\begin{aligned}\alpha_2\,\sigma(t)\, d(\lambda,\beta,V,\omega_r) &\le |\sigma(t)|\,\alpha_2\,|d(\lambda,\beta,V,\omega_r)|\\ &\le |\sigma(t)|\,\alpha_2\bar{\delta}\end{aligned} \tag{B.11}$$

Considering (B.11), (B.10), the following inequality holds:

$$\dot{V} \le -2A_1 V - \sqrt{2}A_2 V^{\frac{1}{2}} \tag{B.12}$$

where $A_1 = b_1$ and $A_2 = b_2 - \alpha_2\bar{\delta}$.

Using (B.12) and according to Lemma 2.1, the time that it takes for V to tend to zero can be calculated as:

$$t_r = t_0 + \frac{1}{A_1}\mathrm{Ln}\left(\frac{2A_1 V(t_0)^{\frac{1}{2}} + \sqrt{2}\,A_2}{\sqrt{2}\,A_2}\right) \tag{B.13}$$

when V converges to zero, based on (B.1), $\sigma(t)$ becomes zero, i.e.:

$$\dot{s}(t) + \frac{k_{2\sigma}}{k_{3\sigma}} s(t) + \frac{k_{1\sigma}}{k_{3\sigma}} s(t)^{\frac{p}{q}} = 0 \tag{B.14}$$

Using (B.14) and Lemma 2.1, the time, that it takes for s to become zero, can be calculated as below:

$$t_{s_1} = t_r + \frac{k_{3\sigma} q}{k_{2\sigma}(q-p)} \mathrm{Ln}\left(\frac{k_{2\sigma}\, s(t_r)^{1-\frac{p}{q}} + k_{1\sigma}}{k_{1\sigma}} \right) \quad (B.15)$$

when S converges to zero, consequently $\dot{s}$ tends to zero and based on (20), it can be deduced that:

$$\dot{s}(t) + \gamma s(t) = k_p\, z(t) + k_I \left(\int_0^t (k_{1I}\, z(\tau)^{\frac{p}{q}} + k_{2I}\, z(\tau))\, d\tau \right) = 0 \quad (B.16)$$

By differentiating (B.16), the following equation is obtained:

$$\dot{z}(t) + \frac{k_{I_1}}{k_p} z(t) + \frac{k_{I_2}}{k_p} z(t)^{\frac{p}{q}} = 0 \quad (B.17)$$

Now, based on Lemma 2.1 and (B.17), the time that it takes for $z(t)$ to become zero, is calculated as:

$$t_s = t_{s_1} + \frac{k_P\, q}{k_{I_2}(q-p)} \mathrm{Ln}\left(\frac{k_{I_2}\, z(t_{s_1})^{1-\frac{p}{q}} + k_{I_1}}{k_{I_1}} \right) \quad (B.18)$$

Since the time derivative of the Lyapunov Function is negative, so it can be concluded that the overall system is stable and all of the closed-loop signals are bounded. Therefore, Δu can be bounded by a positive constant like $\overline{\Delta u}$. It should be noticed that, if a Lyapunov function like $V = \frac{1}{2}\eta(t)^2$ is considered, and if the inequality $b_4 > \frac{\alpha_1}{\alpha_3}\overline{\Delta u}$ holds, according to the Lemma 2.1 and similarly to the previous proof, the auxiliary variable $\eta(t)$ converges to zero in finite-time. When $z(t)$ and $\eta(t)$ tend to zero in finite-time, based on $z(t) = e(t) + \eta(t)$, the speed tracking error $e(t)$ also converges to zero in finite-time t_s and therefore the proof is completed.

REFERENCES

1. Bagheri, P. and Sun, Q., "Adaptive robust control of a class of non-affine variable-speed variable-pitch wind turbines with unmodeled dynamics", ***ISA Transactions***, Vol. 63, (2016), 233-241. (https://doi.org/10.1016/j.isatra.2016.04.008).
2. Kumar, D. and Chatterjee, K., "A review of conventional and advanced MPPT algorithms for wind energy systems", ***Renewable and Sustainable Energy Reviews***, Vol. 55, (2016), 957-970. (https://doi.org/10.1016/j.rser.2015.11.013).
3. Mérida, J., Aguilar, L.T. and Dávila, J., "Analysis and synthesis of sliding mode control for large scale variable speed wind turbine for power optimization", ***Renewable Energy***, Vol. 71, (2014), 715-728. (https://doi.org/10.1016/j.renene.2014.06.030).
4. Hand, M.M., "Variable-speed wind turbine controller systematic design methodology: A comparaison of nonlinear and linear model-based designs", ***National Renewable Energy Laboratory report TP-500-25540***, *National Renewable Energy Laboratory, Golden, CO*, (1999). (https://doi.org/10.2172/12172).
5. Ma, X., "Adaptive extremum control and wind turbine control", Ph.D. thesis, Informatics and Mathematical Modelling, Technical University of Denmark, DTU, DK-2800 Kgs. Lyngby, Denmark, (May 1997).
6. Steinbuch, M., "Dynamic modelling and robust control of a wind energy conversion system", Ph.D. thesis, Delft University of Technology, (November 1989). (ISBN: 90-9003143-X).
7. Bongers, P., "Modeling and identification of flexible wind turbines and a factorizational approach to robust control", Ph.D. thesis, Delft University of Technology, (1994). (ISBN: 90-370-0100-9).
8. Ekelund, T., "Speed control of wind turbines in the stall region", ***Proceedings of IEEE International Conference on Control and Applications (CCA)***, Glasgow, U.K., (1994), 227-232. (https://doi.org/10.1109/CCA.1994.381194).
9. Novak, P., Ekelund, T., Jovik, Y. and Schmidtbauer, B., "Modeling and control of variable-speed wind-turbine drive system dynamics", ***IEEE Control Systems Magazine***, Vol. 15, No. 4, (1995), 28-37. (https://doi.org/10.1109/37.408463).
10. Ebrahimkhani, S., "Robust fractional order sliding mode control of doubly-fed induction generator (DFIG)- based wind turbines", ***ISA Transactions***, Vol. 63, (2016), 343-354. (https://doi.org/10.1016/j.isatra.2016.03.003).
11. Saravanakumar, R. and Jena, D., "Validation of an integral sliding mode control for optimal control of a three blade variable speed variable pitch wind turbine", ***International Journal of Electrical Power & Energy Systems***, Vol. 69, (2015), 421-429. (https://doi.org/10.1016/j.ijepes.2015.01.031).
12. Bossoufi, B., Karim, M., Lagrioui, A., Taoussi, M. and Derouich, A., "Observer backstepping control of DFIG-generators for wind turbines variable-speed: FPGA-based implementation", ***Renewable Energy***, Vol. 81, (2015), 903-917. (https://doi.org/10.1016/j.renene.2015.04.013).
13. Şeker, M., Zergeroğlu, E. and Tatlicioğlu, E., "Non-linear control of variable-speed wind turbines with permanent magnet synchronous generators: A robust backstepping approach", ***International Journal of Systems Science***, Vol. 47, No. 2, (2016), 420-432. (https://doi.org/10.1080/00207721.2013.834087).
14. Moradi, H. and Vossoughi, G., "Robust control of the variable speed wind turbines in the presence of uncertainties: A comparison between H∞ and PID controllers", ***Energy***, Vol. 90, (2015), 1508-1521. (https://doi.org/10.1016/j.energy.2015.06.100).
15. Jafarnejadsani, H., Pieper, J. and Ehlers, J., "Adaptive control of a variable-speed variable-pitch wind turbine using RBF neural network", ***IEEE Transactions on Control Systems Technology***, Vol. 21, No. 6, (2012), 216-222. (https://doi.org/10.1109/TCST.2012.2237518).
16. Saoudi, K. and Harmas, M.N., "Enhanced design of an indirect adaptive fuzzy sliding mode power system stabilizer for multi-machine power systems", ***International Journal of Electrical Power & Energy Systems***, Vol. 54, (2014), 425-431. (https://doi.org/10.1016/j.ijepes.2013.07.034).
17. Eker, I., "Second-order sliding mode control with experimental application", ***ISA Transactions***, Vol. 49, No. 3, (2010), 394-405. (https://doi.org/10.1016/j.isatra.2010.03.010).
18. Pukdeboon, C. and Kumam, P., "Robust optimal sliding mode control for spacecraft position and attitude maneuvers", ***Aerospace Science and Technology***, Vol. 43, (2015), 329-342. (https://doi.org/10.1016/j.ast.2015.03.012).
19. Chiu, C., "Derivative and integral terminal sliding mode control for a class of MIMO nonlinear systems", ***Automatica***, Vol. 48, No. 2, (2012), 316-326. (https://doi.org/10.1016/j.automatica.2011.08.055).
20. Feng, Y., Yu, X. and Man, Z., "Non-singular terminal sliding mode control of rigid manipulators", ***Automatica***, Vol. 38, No. 12, (2002), 2159-2167. (https://doi.org/10.1016/S0005-1098(02)00147-4).
21. Mondal, S. and Mahanta, C., "Adaptive second order terminal sliding mode controller for robotic manipulators", ***Journal of the Franklin Institute***, Vol. 351, No. 4, (2014), 2356-2377. (https://doi.org/10.1016/j.jfranklin.2013.08.027).
22. Feng, Y., Yu, X. and Han, F., "On nonsingular terminal sliding mode control of nonlinear systems", ***Automatica***, Vol. 49, No. 6, (2013), 1715-1722. (https://doi.org/10.1016/j.automatica.2013.01.051).
23. Abolvafaei, M. and Ganjefar, S., "Maximum power extraction from a wind turbine using second-order fast terminal sliding mode control", ***Renewable Energy***, Vol. 139, (2019), 1437-1446. (https://doi.org/10.1016/j.renene.2019.03.044).
24. Azar, A.T. and Serrano, F.E., Design and modelling of anti wind up PID controllers, Complex system modelling and control through intelligent soft computations, Vol. 319, Springer, Switzerland, (2015), 1-44. (https://doi.org/10.1007/978-3-319-12883-2_1).

25. Zhang, X., Zhao, J. and Li, X., "Stability analysis and design of uncertain discrete-time switched systems with actuator saturation using anti-windup and multiple Lyapunov functions approach", ***Asian Journal of Control***, Vol. 19, No. 1, (2017), 325-331. (https://doi.org/10.1002/asjc.1364).
26. Chen, M., Tao, G. and Jiang, B., "Dynamic surface control using neural networks for a class of uncertain nonlinear systems with input saturation", ***IEEE transactions on neural networks and learning systems***, Vol. 26, No. 9, (2014), 2086-2097. (https://doi.org/10.1109/TNNLS.2014.2360933).
27. Edalati, L., Sedigh, A.K., Shooredeli, M.A. and Moarefianpour, A., "Adaptive fuzzy dynamic surface control of nonlinear systems with input saturation and time-varying output constraints", ***Mechanical Systems and Signal Processing***, Vol. 100, (2018), 311-329. (https://doi.org/10.1016/j.ymssp.2017.07.036).
28. Chen, Q., Shi, L., Na, J., Ren, X. and Nan, Y., "Adaptive echo state network control for a class of pure-feedback systems with input and output constraints", ***Neurocomputing***, Vol. 275, (2018), 1370-1382. (https://doi.org/10.1016/j.neucom.2017.09.083).
29. Cui, R., Zhang, X. and Cui, D., "Adaptive sliding-mode attitude control for autonomous underwater vehicles with input nonlinearities", ***Ocean Engineering***, Vol. 123, (2016), 45-54. (https://doi.org/10.1016/j.amc.2016.05.001).
30. Li, Y., Tong, S. and Li, T., "Adaptive fuzzy output-feedback control for output constrained nonlinear systems in the presence of input saturation", ***Fuzzy Sets and Systems***, Vol. 248, (2014), 138-155. (https://doi.org/10.1016/j.fss.2013.11.006).
31. Zhang, Q. and Dong, J., "Disturbance-observer-based adaptive fuzzy control for nonlinear state constrained systems with input saturation and input delay", ***Fuzzy Sets and Systems***, Vol. 392, (2019), 77-92. (https://doi.org/10.1016/j.fss.2019.06.014).
32. Dastres, H., Rezaie, B. and Baigzadehnoe, B., "Neural-network-based adaptive backstepping control for a class of unknown nonlinear time-delay systems with unknown input saturation", ***Neurocomputing***, Vol. 398, (2020), 131-152. (https://doi.org/10.1016/j.neucom.2020.02.070).
33. Qiao, W., Qu, L. and Harley, R.G., "Control of IPM synchronous generator for maximum wind power generation considering magnetic saturation", ***IEEE Transactions on Industry Applications***, Vol. 45, No. 3, (2009), 1095-1105. (https://doi.org/10.1109/TIA.2009.2018914).
34. Torchani, B., Sellami, A. and Garcia, G., "Variable speed wind turbine control by discrete-time sliding mode approach", ***ISA Transactions***, Vol. 1, No. 62, (2016), 81-86. (https://doi.org/10.1016/j.isatra.2016.01.001).
35. Zaafouri, Ch., Torchani, B., Sellami, A. and Garcia, G., "Uncertain saturated discrete-time sliding mode control for a wind turbine using a two-mass model", ***Asian Journal of Control***, Vol. 20, No. 2, (2018), 802-818. (https://doi.org/10.1002/asjc.1594).
36. Errouissi, R., Al-Durra, A. and Debouza, M., "A novel design of PI current controller for PMSG-based wind turbine considering transient performance specifications and control saturation", ***IEEE Transactions on Industrial Electronics***, Vol. 65, No. 11, (2018), 8624-8634. (https://doi.org/10.1109/TIE.2018.2814007).
37. Thomsen, S.C., "Nonlinear control of a wind turbine", MS thesis, Informatics and Mathematical Modelling, Technical University of Denmark, DTU, DK-2800 Kgs. Lyngby, Denmark, (2006).
38. Hoseinzadeh, S., Bahrami, A., Mirhosseini, S.M., Sohani, A. and Heyns, P.S., "A detailed experimental airfoil performance investigation using an equipped wind tunnel", ***Flow Measurement and Instrumentation***, Vol. 72, (2020), 101717. (https://doi.org/10.1016/j.flwmeasinst.2020.101717).
39. Bahrami, A., Hoseinzadeh, S., Heyns, P.S. and Mirhosseini, S.M., "Experimental investigation of co-flow jet's airfoil flow control by hot wire anemometer", ***Review of Scientific Instruments***, Vol. 90, (2019), 125107. (https://doi.org/10.1063/1.5113592).
40. Hammerum, K., "A fatigue approach to wind turbine control", MS thesis, Informatics and Mathematical Modelling, Technical University of Denmark, DTU, DK-2800 Kgs. Lyngby, Denmark, (2006).
41. Colombo, L., Corradini, M.L., Ippoliti, G. and Orlando, G., "Pitch angle control of a wind turbine operating above the rated wind speed: A sliding mode control approach", ***ISA Transactions***, Vol. 96, (2020), 95-102. (https://doi.org/10.1016/j.isatra.2019.07.002).
42. Mobayen, S. and Tchier, F., "Nonsingular fast terminal sliding-mode stabilizer for a class of uncertain nonlinear systems based on disturbance observer", ***Scientia Iranica***, Vol. 24, No 3, (2017), 1410-1418. (https://doi.org/10.24200/SCI.2017.4123).
43. Elbaset, A.A., Mohamed, Y.S., El-Sayed, A.-H.M. and Ahmed, A.E.H.A., Wind driven doubly fed induction generator, Springer, (2018).
44. Jing, X., "Modeling and control of a doubly-fed induction generator for wind turbine-generator systems", MS thesis, Marquett University, Milwaukee, USA, (2012).